Available online at www.elixirpublishers.com (Elixir International Journal)

Vibrational Spectroscopy

Elixir Vib. Spec. 95 (2016) 40950-40960

ISSN: 2229-712X

Scaled Quantum Chemical Calculations and FT-IR, FT-Raman Spectra, Thermo Dynamical Behavior, HOMO-LUMO and Electrostatic Potential Surface Analyses on N,N-Dimethyl-M-Anisidine

M. Murugan[1],V. Balachandran[2], M.Karnan[3], W.Nirmala[1] and MK.Murali[4]

[1]Department of Physics, Government Arts College, Tiruchirappalli 620 022, India.
[2]Department of Physics, A A Government Arts College, Musiri 621 211, India.
[3]Department of Physics, Srimad andavan Arts & Science College, Tiruchirappalli 620 005, India.
[4]Department of Physics, JJ College of Arts & Science , Pudukkottai 622 422, India.

ARTICLE INFO

Article history:
Received: 23 May 2016;
Received in revised form:
9 June 2016;
Accepted: 14 June 2016;

Keywords
FTIR spectra,
FT-Raman spectra,
N,N-dimethyl-m-anisidine,
HOMO-LUMO,
Molecular electrostatic potential (MEP).

ABSTRACT

In this work, the experimental and theoretical vibrational spectra of N,N-dimethyl-m-anisidine (NNDMA, $C_9H_{13}NO$) (3-methoxy-N,N-dimethylaniline) were studied FT-IR and FT-Raman spectra of NNDMA in the liquid phase have been recorded in the region 4000–400 cm^{-1} and 3500–50 cm^{-1}, respectively. The structural and spectroscopic data of the molecule in the ground state have been calculated by using density functional method (B3LYP) with the 6-31G and 6-311++G(d) basis sets. The complete assignments were performed on the basis of the potential energy distribution (PED) of the vibrational modes, calculated with scaled quantum mechanics (SQM) method. The calculated HOMO and LUMO energies show that charge transfer occur in the molecule. Besides, molecular electrostatic potential (MEP) and thermodynamic properties were performed. The other molecular properties like Mulliken population analysis and polarizabilities of NNDMA were reported.

1.Introduction

Anisidines, methoxyanilines, are used as intermediates for the synthesis of azo dyes, pigments and other chemical compounds. Synthesis and properties of the polyanisidines: The oxidative polycondensation of ortho- meta-, and para-anisidines has been studied with cyclic voltammetry and several analytical techniques. During the last decade, attention has been focused on conducting polymers, particularly aromatic polymers such as polyaniline, polypyrrole, [1,2] and polyindole [3]. Excellent optical and electrochemical properties of conducting polymers have led to applications in various areas such as microelectronics [4], gas sensors [5], solar cells [6] and corrosion protection [7]. Among the family of conducting polymers, polyaniline derivatives have received most attention due to their environmental and chemical stability and their ability to switch reversible from insulating state to conducting state [8]. However, the inability of polyaniline to dissolve in common organic solvents has restricted its use in certain fields. The addition of a functional group as a substituent to the polyaniline backbone results in a material, which is more soluble and easily processable. It also possesses the appealing characteristics of polyaniline.While the incorporation of a substituent will increase its solubility and enhance the stability of the polymer product; the electrical conductivity is decreased, due to the increase in electronic localization or reduction in-conjugation.

Despite this, much work remains to be done to understand the properties of these substituted polyanilines so as to apply them technologically [9–14]. Aqueous electrochemical polymerization has been found to be an attractive process for the production of primer coating on metal, which will replace the hazardous method of traditional coating techniques and chromate pretreatment [15]. The advantages of aqueous electropolymerization are (a) the aqueous solutions used are environmentally favorable, b) the technique combines the formation of polymer and deposition of coating in one process and this process can be easily automated, (c) the production cost is relatively low and (d) the properties of the coatings can be controlled by varying the electrochemical parameters [16].

One of the most important applications of conducting polyaniline is its protection of metals against corrosion; Polyaniline has been more extensively studied as anticorrosive coatings on various metals than its derivatives [17]. Regarding the mechanism of corrosion protection by polyaniline, it has been well established that polyaniline has both barrier and electrochemical protection effects. The electrochemical protection is provided by the increase of the corrosion potential and the formation of a protective passive layer on the metal surface due to redox catalytic properties [18].Over the years, various protection methods have been to prevent the degradation processes of Al and its alloys. Aluminum, a very reactive metal, forms a thin solid protecting film of oxide which prevents the further corrosion of the material [19].

Tele: +91 9940788327
E-mail address: phymurugan@gmail.com

Protecting reactive metals like aluminum by covering their surface with an organic coating is a good way of taking advantage of the mechanical property of the metal while protecting them from corrosion. Adhesion of these organic coatings on aluminum is very poor and needs some pretreatment like chromating. Electrodeposition of conducting polymer coatings on aluminum is difficult due to the existence of adherent naturally formed Al_2O_3 [20]. Furthermore, this oxide grows through an anodization process in the acidic solutions normally employed in the electro synthesis of conducting polymers [21, 22].

Density functional theory has been reported [23] and it provides excellent vibrational frequencies of organic compounds if the calculated frequencies are scaled to compensate for the approximate treatment of electron correlation, for the anharmonicity effect [24-26]. In this work, detailed vibrational and electronic structure theory studies of NNDMA were performed using the scaled quantum mechanical (SQM) force field technique based on DFT calculations [27]. The method predicts relatively accurate molecular structure and vibrational spectra with moderate computational effort. The redistribution of electron density (ED) in various bonding and antibonding orbitals and E(2) energies have been calculated by natural bond orbital (NBO) analysis using DFT method to give clear evidence of stabilization originating from the hyperconjugation of various intramolecular interactions. The highest occupied molecular orbital (HOMO) and lowest unoccupied molecular orbital (LUMO) analyses have been used to elucidate information regarding charge transfer within the molecule. In addition, MEP, hyperpolarizability and thermodynamic properties have also been calculated.

2. Experimental Details

The compound NNDMA is obtained from Lancaster Chemical Company, UK and used as such without further purification for the spectral measurements. The Fourier transform infrared spectrum of the title compound was recorded in the region 4000−400 cm^{-1}, at a resolution ±1 cm^{-1}, using BRUKER IFS 66V Vacuum Fourier transform spectrophotometer equipped with an MCT detector, a KBr beam splitter and globar source. The FT−Raman was recorded on the same instrument with an FRA−106 Raman accessory in the region 3500−100 cm^{-1}. The 1064 nm Nd:YAG laser was used as an excitation source, and the laser power was set to 200mW.

3. Computational methods

For a supportive evidence to the experimental observations, the density functional theory (DFT) computations were performed with the aid of GAUSSIAN 09W software package [28] with internally stored B3LYP/6-31G and 6-311++G(d) basis sets. At first, the global minimum energy structure of the title molecule was optimized by both the aforesaid basis set. Subsequently the vibrational normal mode wavenumbers in association with the molecule were derived along with their IR intensity and Raman activity.

In our calculations, there were some deviations persist between the observed and calculated wavenumbers due to the neglect of anharmonic effect at the beginning of frequency calculation and basis set deficiencies. In the present study, these deviations were overcome by a selective scaling procedure in the natural internal coordinate representation followed by the reference [29, 30]. Transformations of the force field and the subsequent normal coordinate analysis including the least squares refinement of the scaling factors, calculation of PED, IR and Raman intensities were done on a PC with the MOLVIB program (Version V7.0-G77) written by Sundius [31□33]. The PED elements provide a measure of each internal coordinate's contribution to the normal coordinate. For the plots of simulated IR and Raman spectra, pure Lorentzian band shapes were used with a bandwidth of 10 cm^{-1} and the modified Raman activities during scaling procedure with MOLVIB were converted to relative Raman intensities using the following relationship derived from the basic theory of Raman scattering [34-36].

$$I_i = \frac{f(\upsilon_0 - \upsilon_i)^4 S_i}{\upsilon_i \left[1 - \exp\left(\frac{-hc\upsilon_i}{kT}\right)\right]}$$

where υ_0 is the exciting wavenumber (1064 nm = 9398 $cm\upsilon 1$) of laser light source used while recording Raman Spectra, υ_i the vibrational wavenumber of the ith normal mode, h, c and kb fundamental constants, and f is a suitably chosen common normalization factor for all peak intensities of the Raman spectrum of the title molecule. Finally, the converted Raman intensities and the calculated infrared intensities were modified by assigning the highest intensity peak to 100%.

In order to predict the reactive behavior of a molecule, we have plotted MEP surface and derived electrostatic potential values and point charges at B3LYP/6-31G and 6-311++G(d) basis sets. The population of atomic charges on the individual atoms and the distribution of atomic charges in core and valance were also derived using NBO calculations in GAUSSIAN 09W. From the computed NBO results, the stabilization energies of molecular species which are most responsible for the stability of molecule were identified. Furthermore, the highest occupied molecular orbital (HOMO) and the lowest unoccupied molecular orbital (LUMO) energies were predicted to interpret the orbital overlapping and the possibility of charge transfer within the molecule using B3LYP/6-31G method and basis set combination. Apart from the aforesaid calculations, certain thermodynamic properties were computed at B3LYP/6-311++G (d,p) method to examine the intensity of molecular vibrations at different temperatures.

4. Results and discussion

4.1Optimized geometrical parameters and Natural atomic orbitals

The most optimized geometries are performed by B3LYP methods with atoms numbering are shown in Fig 1. The optimized bond lengths, bond angles and dihedral angles of title compound which are calculated by DFT methods B3LYP/6-31G and 6-311++G(d) basis sets are shown in Table 1.

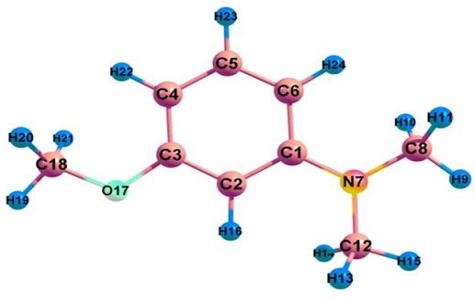

Fig1. Geometrical optimized structure of NN dimethyil-m-anisidine.

Table 1. Optimized geometrical parameters of NN dimethyil-m-anisidine at B3LYP / 6-31+G and B3LYP / 6-311++G(d)

Parameters	B3LYP 6-31+G	B3LYP / 6-311++G(d)	Parameters	B3LYP / 6-31+G	B3LYP / 6-311++G(d)
C1-C2	1.411	1.406	C2-C1-C6	118.055	0.003
C1-C6	1.421	1.417	C2-C1-N7	120.836	-179.996
C1-N7	1.393	1.384	C6-C1-N7	121.110	-179.998
C2-C3	1.398	1.396	C1-C2-C3	120.623	0.003
C2-H16	1.081	1.082	C1-C2-H16	122.077	-0.001
C3-C4	1.400	1.397	C3-C2-H16	117.300	179.998
C3-O17	1.397	1.370	C2-C3-C4	121.435	-180.000
C4-C5	1.401	1.396	C2-C3-O17	114.629	-0.001
C4-H22	1.082	1.082	C4-C3-O17	123.936	-179.997
C5-C6	1.392	1.386	C3-C4-C5	117.808	0.002
C5-H23	1.086	1.086	C3-C4-H22	121.887	0.003
C6-H24	1.082	1.082	C5-C4-H22	120.305	-179.999
N7-C8	1.460	1.450	C4-C5-C6	121.955	-0.003
N7-C12	1.460	1.450	C4-C5-H23	119.089	179.990
C8-H9	1.091	1.089	C6-C5-H23	118.956	179.996
C8-H10	1.100	1.097	C1-C6-C5	120.124	-0.011
C8-H11	1.100	1.097	C1-C6-H24	120.593	0.000
C12-H13	1.100	1.097	C5-C6-H24	119.284	179.994
C12-H14	1.100	1.097	C1-N7-C8	120.181	-179.992
C12-H15	1.091	1.089	C1-N7-C12	119.983	0.001
O17-C18	1.449	1.418	C8-N7-C12	119.835	179.905
C18-H19	1.090	1.089	N7-C8-H9	109.139	-0.102
C18-H20	1.097	1.095	N7-C8-H10	111.917	0.003
C18-H21	1.097	1.095	N7-C8-H11	111.917	179.999
			H9-C8-H10	107.947	-179.991
			H9-C8-H11	107.947	0.005
			H10-C8-H11	107.820	-0.002
			N7-C12-H13	111.832	179.999
			N7-C12-H14	111.831	-179.999
			N7-C12-H15	109.230	0.003
			H13-C12-H14	107.767	179.997
			H13-C12-H15	108.018	-60.725
			H14-C12-H15	108.018	60.719
			O17-C18-H19	105.251	119.276
			O17-C18-H20	111.410	-119.280
			O17-C18-H21	111.409	-60.646
			H19-C18-H20	109.667	60.631
			H19-C18-H21	109.665	179.993
			H20-C18-H21	109.359	119.353

The absence of the imaginary frequencies as well as of negative eigen values of the second-derivative matrix confirmed that the stationary point obtained in this study corresponds to the minima of potential energy hyper surfaces. Kydd *et.al* suggested that the electron withdrawing CH_3 group substitution enhances the delocalization of electron density (ED) [37]. In order to prove the enhancement of CH_3 group, the natural atomic orbital (NAO) occupancies and their energies of NNDMA are computed at B3LYP/6-311+G (d, p) basis set method. In this present work, geometry optimization parameters for NNDMA have been employed without symmetry constrain from Table 1.

4.2 Vibrational assignments

The molecule under consideration would belong to Cs point group and the 66 normal mode of fundamental vibrations, which span the irreducible representation 45A′+21A″. The A′ modes are polarized while the A″ modes are depolarized in the Raman spectrum.

All the calculated modes of vibrations are numbered from the smallest to largest within each fundamental wavenumber. The observed FT-IR and FT-Raman bands for various modes of vibrations are assigned and presented in the Table 2. Comparison of the vibraional modes calculated at B3LYP with experimental values (Table 2) reveals that over estimation of the calculated vibraional modes due to neglect of anharmonicity in the real system. The observed and simulated FT-IR and FT-Raman spectra of NNDMA at (B3LYP) with the 6-31G and 6-311++G(d) basis sets are shown in Figs. 2 and 3, respectively. The calculated vibrational wavenumbers are usually higher than the corresponding experimental quantities because of the combination of electron correlation effects and basis set deficiencies. Therefore, it is customary to scale down the calculated harmonic wavenumbers in order to improve the agreement with the experiment. In the present case, we have followed four different scaling factors.

Table 2 . Vibrational spectral analysis of N,N-dimethyl-m-anisidine based on B3LYP/6-31G and B3LYP /6-311++G(d)

Mode No.	Sym. Spe.	Observed frequencies (cm^{-1})		Calculated frequencies (cm^{-1})				Infrared intensity		Raman activity		Vibrational assignments/ (%)PED
		FT-IR	FT-Raman	Unscaled		Scaled		A	B	A	B	
				A	B	A	B					
1			3083	3260	3217	3084	3081	3.30	3.98	64.83	63.97	νCH(99)
2		3045		3248	3214	3047	3046	10.02	8.26	127.57	117.65	νCH(98)
3			3024	3242	3209	3026	3024	19.02	15.48	49.28	52.55	νCH(98)
4			2952	3194	3162	2955	2953	18.26	17.32	90.86	94.24	νCH(96)
5		2909		3174	3135	2912	2911	25.13	46.34	123.96	181.64	νassCH3(99)
6			2833	3158	3135	2833	2832	47.53	34.00	163.86	118.51	νassCH3(99)
7		2818		3144	3119	2820	2819	2.79	2.49	1.64	0.56	νassCH3(99)
8			2786	3099	3067	2787	2785	48.15	46.22	60.78	63.92	νassCH3(98)
9				3053	3027	2712	2711	93.36	97.97	22.21	39.77	νassCH3(98)
10				3050	3027	2700	2698	8.51	7.03	135.66	190.79	νassCH3(98)
11				3030	3009	2692	2691	53.19	65.21	139.70	164.16	νssCH3(98)
12				3012	2996	2683	2682	46.28	50.19	262.81	350.06	νssCH3(98)
13				3003	2987	2667	2664	107.63	125.70	32.53	42.73	νssCH3(97)
14		1644		1675	1654	1645	1643	289.39	337.40	43.26	52.24	νCC(72),δCH(12)
15		1604	1607	1627	1610	1606	1607	82.28	108.80	14.41	20.65	νCC(70),δCH(16)
16		1548		1577	1551	1550	1549	106.79	139.63	19.85	7.37	νCC(72),δCH(18)
17				1566	1538	1515	1514	11.46	37.30	0.65	2.75	νCC(71),δCH(16)
18				1561	1534	1503	1501	61.72	20.89	5.01	2.44	νCC(75),δCH(13)
19		1467		1547	1521	1469	1468	25.62	24.01	15.61	7.29	δopbCH3(85)
20			1452	1534	1509	1452	1451	12.11	15.48	45.92	18.72	δopbCH3(86)
21				1532	1508	1447	1446	6.88	6.80	34.83	17.19	δopbCH3(86)
22				1530	1505	1441	1440	35.09	29.94	6.15	3.83	δsbCH3(85)
23				1525	1501	1439	1437	0.04	0.01	12.60	9.59	δsbCH3(88)
24		1433		1510	1488	1435	1434	9.68	19.91	6.68	7.06	δsbCH3(80)
25		1411		1496	1482	1412	1410	8.35	10.30	17.34	4.22	δipbCH3(80)
26			1351	1492	1462	1352	1352	1.84	1.50	27.19	14.95	δipbCH3(83)
27		1322		1406	1388	1324	1323	64.69	91.59	10.84	17.16	δipbCH3(83)
28		1300	1304	1391	1364	1304	1303	37.39	34.97	4.43	5.62	νCN(77),δring(16)
29		1278		1370	1347	1279	1277	6.44	7.74	3.62	5.93	νCN(81)
30			1238	1297	1291	1240	1239	92.40	191.69	2.73	6.22	νCC(80)
31		1222		1267	1253	1223	1221	76.61	87.53	12.04	8.38	δCH(66),νCN(16),δCO(10)
32			1179	1236	1215	1181	1180	37.59	4.30	1.57	6.31	νCN(71)
33		1133		1213	1205	1134	1133	55.39	25.46	7.97	1.95	νCO(65), δCH(16),δipb(12)
34				1186	1178	1104	1102	95.31	0.78	7.07	3.29	νCO(73)
35			1095	1168	1178	1097	1095	0.00	152.43	6.44	4.20	νCN(70)
36		1078		1165	1153	1078	1077	0.29	0.00	8.01	1.88	δCH(65)
37		1066		1163	1144	1068	1067	0.18	0.03	2.51	1.02	δrockCH3(66),δCH(19)
38			1012	1141	1123	1016	1014	2.24	2.74	3.34	4.52	δCH(66)

39		967		1096	1088	968	965	32.25	36.50	0.39	0.43	δrockCH3(87),
40		933		1063	1084	936	935	94.60	52.81	1.39	1.42	δrockCH3(87),
41			851	1028	1012	852	852	5.32	15.27	37.70	26.24	γrockCH3(85)
42		828		984	983	829	827	0.55	1.03	1.31	32.89	γringCH3(55),δCN(18),δCO (13)
43		800		983	930	803	801	0.05	0.04	6.21	0.28	δCH(80)
44			762	872	869	764	763	43.63	6.09	1.33	2.20	δCO(66),δCH(12),νCN(10)
45		733		862	840	733	732	4.41	39.74	2.10	0.44	γCH(60),γCO(14),γring(10)
46			702	861	810	703	702	11.20	2.11	1.14	0.25	γCH(68),γring(16)
47		678		784	745	681	679	49.59	35.66	2.08	1.14	γCH(66),γring(18)
48			631	727	720	633	632	3.95	4.40	15.86	14.94	γring(72),γCN(11),γCO(10)
49		622		709	693	623	621	11.74	28.60	0.15	0.03	γCH(70),γring(20)
50			583	642	632	585	584	0.08	0.01	0.04	2.17	γring(70),γCO(12),γCN(10)
51		567		585	585	569	568	11.16	10.04	1.70	0.49	δCN(57),δring(21),
52			524	565	558	526	525	3.43	1.45	2.24	1.55	δCN(58),δCH(19)
53			476	528	521	477	475	0.87	1.19	1.30	1.39	δCN(55),δCH(20)
54		453	451	477	459	453	451	1.11	4.58	0.31	0.10	δring(48),νCN(19)
55			382	424	420	383	381	0.93	1.16	2.91	3.10	δCN(58),δring(21)
56				356	354	301	299	0.20	0.47	8.78	9.33	δring(43), γCN (18)
57				295	291	265	264	4.66	1.82	0.19	1.55	δring(54),γCO(21)
58				286	275	213	212	2.39	0.01	1.00	0.01	ΓCH3(71), γCO(12)
59				275	271	186	184	1.65	0.65	0.73	0.05	ΓCH3(70), γCO(10)
60				223	225	163	162	0.14	0.21	0.16	0.24	ΓCH3(70), γCN(12),γCO(10)
61				191	187	160	158	0.39	0.06	2.02	2.50	γCO(40),γCN(27)
62				178	180	135	134	2.58	2.16	0.63	0.42	γCN(37),γCO(19),γring(10)
63				150	151	124	123	0.18	0.59	3.80	3.39	γCO(40),γCN(20),γring(12)
64				93	90	72	70	0.00	5.68	0.02	0.21	γCN(35),γCO(19),γring(12)
65				80	75	65	66	9.57	0.42	0.62	0.28	γCN(39),γCO(18),γring(10)
66				60	54	45	43	3.17	2.06	0.23	1.06	γCN(35),γCO(17),γring(11)

A: B3LYP/6-31G; B: B3LYP/ 6-311++G(d)

4.2 Vibrational assignments

The molecule under consideration would belong to Cs point group and the 66 normal mode of fundamental vibrations, which span the irreducible representation 45A′+21A″. The A′ modes are polarized while the A″ modes are depolarized in the Raman spectrum. All the calculated modes of vibrations are numbered from the smallest to largest within each fundamental wavenumber. The observed FT-IR and FT-Raman bands for various modes of vibrations are assigned and presented in the Table 2. Comparison of the vibraional modes calculated at B3LYP with experimental values (Table 2) reveals that over estimation of the calculated vibraional modes due to neglect of anharmonicity in the real system. The observed and simulated FT-IR and FT-Raman spectra of NNDMA at (B3LYP) with the 6-31G and 6-311++G(d) basis sets are shown in Figs. 2 and 3, respectively. The calculated vibrational wavenumbers are usually higher than the corresponding experimental quantities because of the combination of electron correlation effects and basis set deficiencies. Therefore, it is customary to scale down the calculated harmonic wavenumbers in order to improve the agreement with the experiment. In the present case, we have followed four different scaling factors.

It is convenient to discuss the vibrational spectra of NNDMA in terms of characteristic spectral regions as described below:

C−H vibrations

Aromatic compounds commonly exhibit multiple weak bands in the region 3100−3000cm^{-1} due to aromatic C−H stretching vibration [38, 39]. They are not appreciably affected by the nature of the substituents. In the present study, the band 3045 cm^{-1} are assigned to C−H stretching vibration in FT-IR and corresponding FT-Raman vibration are ascribed at 3083, 3024 and 2952 cm^{-1}. The observed wavenumbers of C−H stretching vibration are also in good agreement with the measured values and literature data [40]. The C−H in-plane and out-of-plane bending vibrations generally lie in the region 1300−1000 cm^{-1} and 1000−675 cm^{-1} [41, 42], respectively. In accordance with above literature data, the weak band observed in FT-Raman and FT-IR spectrum at 1222, 1078, 1012 and 800 cm^{-1} are assigned to C−H in-plane bending vibration with minor contribution of C-C-C stretching vibration. They show good agreement with the theoretically computed values at 1221,1077, 1014 and 829 cm^{-1} by (B3LYP) with the 6-31G and 6-311++G(d) basis sets. The bands observed at 733, 678, 622 and 702 cm^{-1} in the FT-IR and FT-Raman modes are assigned to C−H out-of-plane bending vibration of NNDMA. The corresponding theoretically computed values are presented in Table 2.

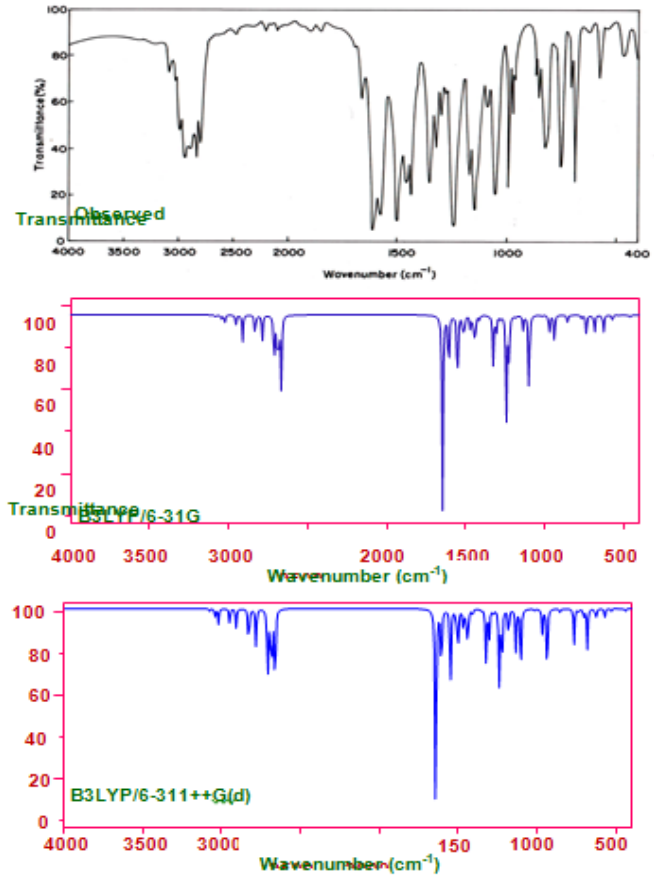

Fig. 2. Observed FT-IR and simulated spectrum of NN dimethyil-m-anisidine.
(a) Observed (b) B3LYP/6-3G (c) B3LYP/6-311++G(d).

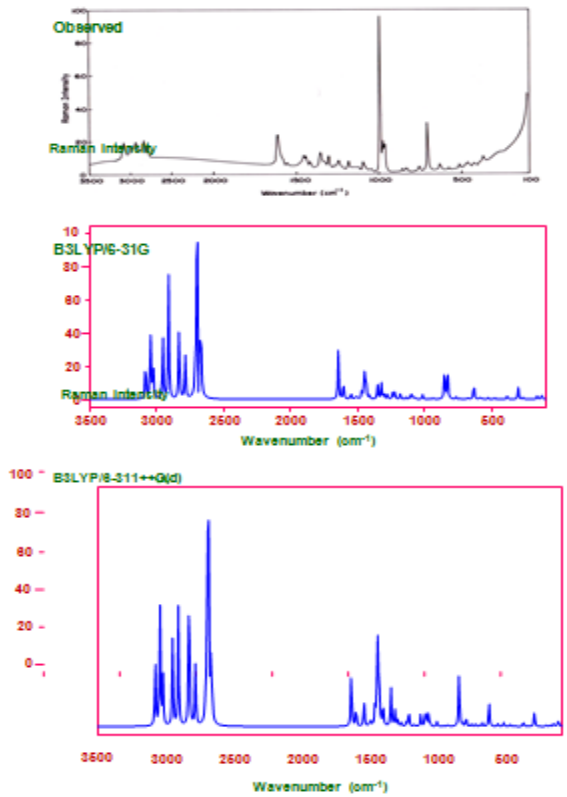

Fig 3. Observed FT-IR and simulated spectrum of NN dimethyil-m-anisidine.Observed (b) B3LYP/6-31G (c) B3LYP/6-311++G(d).

CH_3 Vibrations

The title molecule NNDMA under consideration possesses a trible CH_3 group. For the assignments of CH_3 group frequencies, are can expect nine fundamentals can be associated to each CH_3 group, namely the asymmetrical stretching (CH_3ass), symmetrical stretching (CH_3ss), in-plane bending (CH_3ipb), out-of-plane bending (CH_3opb), symmetric bending (CH_3sb), the in-plane rocking (CH3ipr), out-of-plane rocking (CH3opr) and twisting mode in CH_3 (CH_3twist). Methyl groups are generally referred as electron donating substitution in the aromatic ring system [43]. In aromatic compounds, the CH3 asymmetric stretching vibrations occurs at values greater than 3000 cm^{-1} and CH3 symmetric stretching vibrations occurs at values just below than 3000 cm^{-1} [44]. The CH methyl group stretching vibrations are generally observed in the range of 3000–2800 cm^{-1} [45, 46]. The above results from the asymmetric stretching CH3 mode in which the two C–H bonds of the methyl group are extending while the third one is contracting it is symmetric stretching mode, in which all the three C–H bonds extend and contract in phase. In the present case, the FT-IR and FT-Raman band at 2909, 2818, 2833 and 2786 cm^{-1} represent asymmetric stretching mode. The calculated asymmetric modes are 2911, 2818, 2832 and 2785 cm^{-1} at B3LYP /6-311++G(d) method good agreement with observed data's. The symmetric mode was calculated at 2691, 2682 and 2664 cm^{-1} by B3LYP/6-311++G(d) method, respectively with PED contribution of 95%.

Three bending modes can occur within a methyl group. The first of these, the symmetric bending vibration, involves the in-phase bending of C–H bonds. The second the asymmetric bending vibration, involves out-of-phase bending of the C–H bonds. For NNDMA, the values observed at 1411, 1322 cm^{-1} in FT-IR and 1351 cm^{-1} in FT-Raman spectrum are attributed to CH_3 in-plane bending vibrations. The out-of-plane bending modes are calculated at 1467 and 1452 cm^{-1} in FT-IR and FT-Raman spectrum. Methyl rocking frequencies are mass sensitive and variable in position due to the interaction with skeletal stretching modes [47]. Generally, these bands are observed in the range 1120–1050 cm^{-1} and 900–800 cm^{-1} [48, 49]. In the present molecule, the FT-IR and FT-Raman spectrum shows the bands at 1066, 967, 933 cm^{-1} assigned in in-plane rocking and 851 cm^{-1} in out-of-plane rocking vibrations. As CH_3 twisting mode is expected below 400 cm^{-1}, the computed bands at 212, 184 and 162 cm^{-1} in B3LYP /6-311++G(d) method with basis set, respectively, are assigned to mode, for, no spectral measurements were possible in the region due to instrumental limits.

C–N vibrations

The C–N stretching frequency is a rather hard job since there are problems in identifying these frequencies from other vibrations. The C–N stretching absorption for aromatic amines are identified in the region 1382–1266 cm^{-1} [50]. In the present study, the C–N stretching vibrations are observed only at 1300, 1278, 1304, 1179 and 1095 cm^{-1} in FT-IR and FT-Raman spectrum is good agreement with the experimental values 1303, 1277, 1181 and 1095 cm^{-1} in B3LYP/6-311++G(d) method with 6-311G (d) basis set. According to the literature, one band is more deviated since the C–N bond is in between ring and NO_2. All the bands lie in the expected range when compared to the literature [51]. Consequently, the C–N in-plane and out-of-plane bending vibrations assigned at 567, 524, 470 and 382 cm^{-1} in FT-IR and FT-Raman spectrum. These assignments are validated by the literature [52–54]. The identification of C–N vibration is a difficult task since, it falls in a complicated region of the vibrational spectrum. However, with the help of force field calculations, the C–N vibrations were well identified and assigned in this study.

C–O vibrations

The C–O stretching vibrations in NNDMA [55] occur as a strongest band in the region 1300–1200 cm^{-1}.The C–O stretching mode may be coupled with the adjacent C–C stretching modes [56]. The C–O stretching vibration of the title compound is observed at 1133 cm^{-1} in FT-IR. The in-plane and out-of-plane bending vibrations have also been identified and presented in Table 2.

C-C vibrations

The ring carbon-carbon stretching vibrations occur in the region 1625-1430 cm^{-1}. For aromatic six member rings, e.g., benzene and pyridines, there are two or three bands in this region due to skeletal vibrations, the strongest usually being at about 1500 cm^{-1}. In the case where the ring is conjugated further band at about 1580 cm^{-1} is also observed. In general, the bands are of variable intensity and are observed in the regions 1625-1590, 1590-1575, 1525-1470 and 1465-1430 cm^{-1}. For the substituted benzenes with identical atoms or groups on all para-pair of ring carbon atoms, the vibrations causing the bands at 1625-1590 cm^{-1} are infrared-inactive due to symmetry considerations the compound having a centre of symmetry at the ring centre. If the groups on a para-pair of carbon atoms are different them there is no centre of symmetry and vibrations are infrared active [57]. Based on the above literature data, in our present study the medium and strong bands observed at 1644, 1604, 1607, 1548, 1238 cm^{-1} in FT-IR and FT Raman spectrum are assigned to C-C stretching vibrations. The theoretical values by B3LYP/6-311++G(d) level show satisfactory agreement with recorded spectral data.

4.3 Natural population analysis

The natural population analysis [58] performed on the title molecule clearly describes the distribution of charges in the various sub-shells (core, valence, Rydberg) in the molecular orbital. The accumulation of natural charges on individual atom of the title molecule is given in Table 3. It shows that an atom C5 has the most electronegative charge of -0.159e and C3 has the most electropositive charge of 0.323e. Likewise, C2, C4, C5, C6, N7, C8, C12, O17 and C18 atoms have considerable electro negativity and they are tending to donate an electron. Conversely, all hydrogen atoms have considerable electropositive and they are tending to acquire an electron.

Core	: 49.99139 (99.9828% of 50)
Valence	: 65.78540 (99.6748% of 66)
Rydberg	: 0.22321 (0.1924% of 116)

4.4 Analysis of Molecular electrostatic potential (MEP) surface.

The MEP surface generally provides information regarding the chemical reactivity of a molecule. The electrostatic potential generated in space around a molecule by the charge distribution is helpful to understand how much electrophilic or nucleophilic the molecular species is. The electrostatic potential $V(\vec{r})$ at any point in space around a molecule by charge distribution is given by

$$V(\vec{r}) = \sum_A \frac{Z_A}{\left|\vec{R}_A - \vec{r}\right|} - \int \frac{\rho(\vec{r}')\,dr'}{\left|\vec{r}' - \vec{r}\right|}$$

Where $\rho(\vec{r}')$ is the electron density function of the molecule, ZA is the charge on the nucleus A located at $\vec{R}_A$ and $\vec{r}$ is the dummy integration variable. $V(\vec{r})$ is a real physical property, which can be determined either computationally or experimentally by diffraction methods [59].

Fig. 4 shows the plot of MEP surface of NNDMA along with the computationally derived electrostatic potential and electrostatic point charges on its individual atoms. In the colour scheme of MEP, the intensity of which is proportional to the absolute value of the potential energy. On the other hand, the positive electrostatic potentials are appeared as blue and the Green indicates surface areas where the potentials are closer to zero.

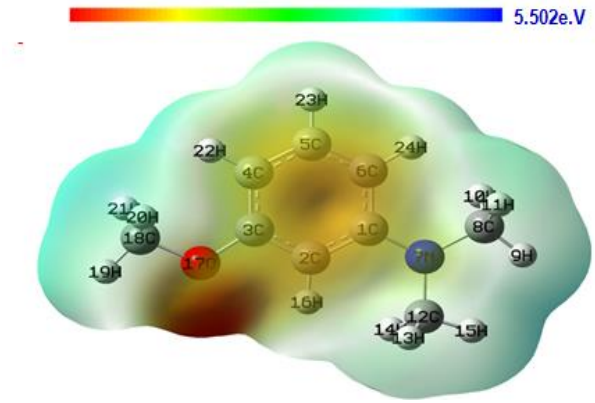

Fig 4. 3D-Molecular electrostatic potential map of NN dimethyil-m-anisidine.

4.5 Frontier molecular orbitals (FMOs)

The analysis of FMOs describes one electron excitation from the highest occupied molecular orbital (HOMO) to the lowest unoccupied molecular orbital (LUMO). The energy of HOMO is directly related to the ionization potential and the energy of LUMO is related to the electron affinity. The HOMO–LUMO energy gap is an important stability index and it also reflects the chemical activity of a molecule [60]. The molecular orbitals are defined as eigen functions of the Fock operator, which exhibits the full symmetry of the nuclear point group, they necessarily form a basis for irreducible representations of full point-group symmetry. The energies of HOMO, HOMO–1, HOMO–2, LUMO, LUMO+1 and LUMO+2 and their orbital energy gaps calculated at B3LYP/6-311++G (d) method and the pictorial illustration of the FMOs and their respective positive and negative regions are shown in Fig. 5.

In the HOMO surface, the bonding π orbitals spreading over the ring carbon atoms are helpful to hold the molecule together. It is worth mentioning here that the molecular orbital lobes located over the chlorine atom of HOMO surface is a non-bonding orbital. Hence the electrons in chlorine atom are acts little like a lone pairs of electrons in a Lewis structure. In contrast the molecular orbital lobes spreading over C2–H11 and C5–H17 bonds are σ orbitals and they have cylindrical symmetry about the internuclear axis. The same type of σ orbital is also identified on the bond C3–H12 in LUMO+1 surface. The molecular orbital lobes spreading over the HOMO–2 and LUMO+2 surfaces are of ant bonding character because it has a node between adjacent nuclei with lobes of opposite sign (shown in different colours) and p-orbital on the chlorine atom is a major contributor of HOMO–2, LUMO+2 surfaces. The energy gap between HOMO and LUMO explains the eventual charge transfer interaction within the molecule, which influences the biological activity of the molecule.

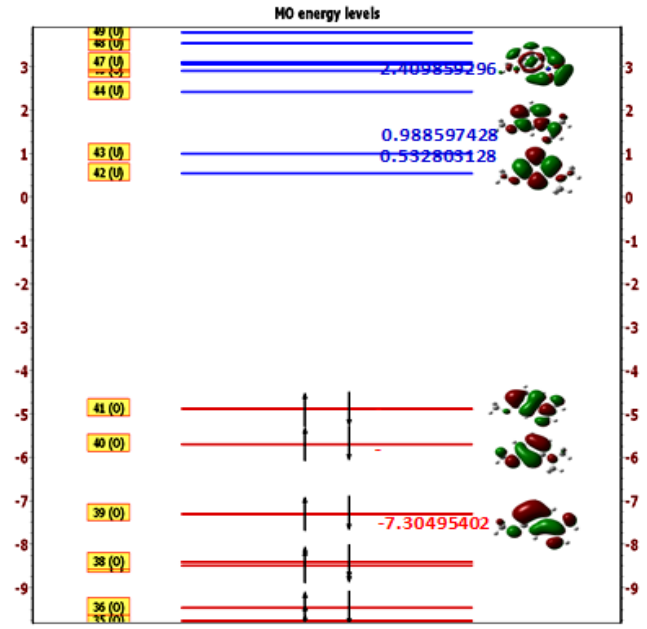

Fig 5. The atomic orbital composition of the frontier molecular orbital for NN dimethyil-m-anisidine

4.6 Mulliken atomic charge

Mulliken atomic charge calculation has an important role in the application of quantum chemical calculation to molecular system because of atomic charges effect dipole moment, molecular polarizability, electronic structure and more a lot of properties of molecular systems. The calculated Mulliken charge values of NNDMA are listed in Table 4. The Mulliken charge distribution of the NNDMA in (B3LYP)

Table 3. Natural population analysis of NN dimethyil-m-anisidine.

Atom No	Natural Charge	Natural Population			
		Core	Valence	Rydberg	Total
C1	0.196	1.999	3.791	0.014	5.804
C2	-0.308	1.999	4.296	0.013	6.308
C3	0.323	1.999	3.662	0.017	5.677
C4	-0.333	1.999	4.322	0.012	6.333
C5	-0.159	1.999	4.147	0.013	6.159
C6	-0.282	1.999	4.271	0.012	6.282
N7	-0.453	1.999	5.446	0.008	7.453
C8	-0.352	1.999	4.345	0.008	6.352
H9	0.193	0.000	0.806	0.001	0.807
H10	0.180	0.000	0.817	0.003	0.820
H11	0.180	0.000	0.817	0.003	0.820
C12	-0.353	1.999	4.346	0.008	6.353
H13	0.181	0.000	0.816	0.003	0.819
H14	0.181	0.000	0.816	0.003	0.819
H15	0.192	0.000	0.807	0.001	0.808
H16	0.222	0.000	0.776	0.003	0.779
O17	-0.525	2.000	6.520	0.005	8.525
C18	-0.212	1.999	4.204	0.009	6.212
H19	0.187	0.000	0.812	0.001	0.813
H20	0.165	0.000	0.833	0.002	0.835
H21	0.164	0.000	0.833	0.002	0.836
H22	0.208	0.000	0.790	0.002	0.792
H23	0.200	0.000	0.798	0.002	0.800
H24	0.205	0.000	0.793	0.002	0.795

Table 4. Mulliken population analysis of NN dimethyil-m-anisidine performed at B3LYP/6-31G and B3LYP /6-311++G(d)

Atoms	Atomic charges	
	B3LYP/ 6-31G	B3LYP / 6-311++G(d)
C1	0.339	-0.749
C2	-0.166	-0.978
C3	0.267	0.149
C4	-0.135	0.586
C5	-0.152	-0.846
C6	-0.146	0.491
N7	-0.632	0.392
C8	-0.229	-0.744
H9	0.140	0.210
H10	0.150	0.242
H11	0.150	0.242
C12	-0.228	-0.805
H13	0.152	0.250
H14	0.152	0.250
H15	0.138	0.218
H16	0.131	0.295
O17	-0.568	-0.069
C18	-0.164	-0.633
H19	0.163	0.262
H20	0.145	0.242
H21	0.145	0.242
H22	0.117	0.250
H23	0.116	0.263
H24	0.114	0.238

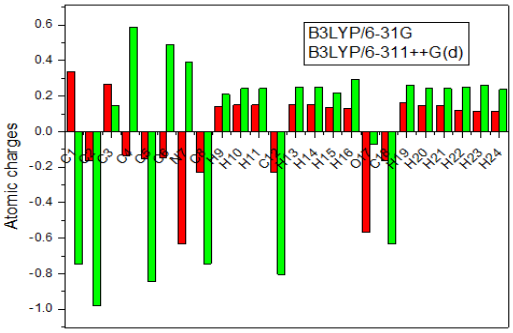

Fig 6. Correlation graph of Mulliken atomic charges with B3LYP/6-31G and B3LYP/6-311++G(d) methods.

with the 6-31G and 6-311++G(d) basis sets are shown in Fig. 6. The charge distribution of the titled molecule shows all the hydrogen atoms and C1, C3 are positively charged whereas the other carbon atoms are negative. The influence of electronic effect resulting from the hyperconjugation and induction of methylene group in the aromatic ring causes a large negatively charged value in the carbon atom C12 in NNDMA. The charge changes with basis set presumably occurs due to polarization. All hydrogen atoms are positive charges in title compound.

4.7 Hyperpolarizability calculations

The polarizability α and the hyper polarizability β and the electric dipole moment μ of the NNDMA are calculated by finite field method using (B3LYP) with the 6-31G and 6-311++G(d) basis sets are available in DFT package. To calculate all the electric dipole moments and the first hyper polarizabilities for the isolated molecule, the origin of the Cartesian coordinate system (x,y,z)=(0,0,0) was chosen at own centre of mass of NNDMA.

The first hyperpolarizability (β0) of this noval molecular system and related properties (β, α0 and Δα) of NNDMA are calculated and it is based on the finite-field approach. In the presence of an applied electric field, the energy of a system is a function of the electric field. First hyperpolarizability is a third rank tensor that can be described by a 3x3x3 matrix. The 18 components of the 3D matrix can be reduced to 10 components due to the Kleinman symmetry [61]. It can be given in the lower tetrahedral format. It is obvious that the lower part of the 3x3x3 matrixes is a tetrahedral. The components of β are defined as the coefficients in the Taylor series expansion of the energy in the external electric field. When the external electric field is weak and homogeneous, this expansion becomes:

$$E = E^0 - \mu_\alpha F_\alpha - \tfrac{1}{2}\alpha_{\alpha\beta}F_\alpha F_\beta - \tfrac{1}{6}\beta_{\alpha\beta\gamma}F_\alpha F_\beta F_\gamma + ...$$

where E0 is the energy of the unperturbed molecules, Fα is the field at the origin μα, ααβ and βαβγ are the components of dipole moment, polarizability and the first hyperpolarizability, respectively. The total static dipole moment μ, the mean polarizability α0, the anisotropy of the polarizability Δα and the mean first hyperpolarizability β0, using the x,y,z components they are defined as:

$$\mu = \left(\mu_x^2 + \mu_y^2 + \mu_z^2\right)^{1/2}$$

$$\alpha_0 = \frac{\alpha_{xx} + \alpha_{yy} + \alpha_{zz}}{3}$$

$$\alpha = 2^{-1/2}\left[(\alpha_{xx} - \alpha_{yy})^2 + (\alpha_{yy} - \alpha_{zz})^2 + (\alpha_{zz} - \alpha_{xx})^2 + 6\alpha_{xx}^2\right]^{1/2}$$

$$\beta_0 = \left(\beta_x^2 + \beta_y^2 + \beta_z^2\right)^{1/2}$$

$$\beta_x = \beta_{xxx} + \beta_{xyy} + \beta_{xzz}$$

$$\beta_y = \beta_{yyy} + \beta_{xxy} + \beta_{yzz}$$

$$\beta_z = \beta_{zzz} + \beta_{xxz} + \beta_{yyz}$$

The HF and DFT/6-311++G (d, p) calculated first hyperpolarizability of NNDMA 6.018839×10-30 and 4.362984×10-30 esu, are shown in Table 5.

4.8 Thermodynamic properties

The total energy of a molecule is the sum of translational, rotational, vibrational and electronic energies. ie, E = Et + Er + Ev + Ee. The statistical thermo chemical analysis of NNDMA is carried out considering the molecule to be at room temperature of 298.15 K and one atmospheric pressure. The thermodynamic parameters, like rotational constant of the molecule by DFT (B3LYP level) and method is presented in Table 6 for NNDMA. The title molecule is considered as an asymmetric top having rotational symmetry number 1 and the total thermal energy has been arrived as the sum of electronic, translational, rotational and vibrational energies.

The variations in the zero point vibrational energy seem to be insignificant. The thermodynamic functions are determined from spectroscopic data by statistical methods. The thermodynamic quantities such as entropy Svib, enthalpy (H−E)/T, and Gibb's free energy (G–E)/T for various ranges (100K-1000K) of temperatures are determined using the vibrational wave numbers and these results are presented in the Table 6.

Table 5 .The B3LYP/6-31G and B3LYP /6-311++G(d) calculated electric dipole moments (Debye), Dipole moments compound, polarizability (in a.u), β components and β_{tot} (10^{-30} esu) value of NN dimethyil-m-anisidine.

Parameters	B3LYP/ 6-31G	B3LYP/ 6-311++G(d)	Parameters	B3LYP/ 6-31 G	B3LYP/ 6-311++G(d)
μ_x	0.879	0.912	β_{xxx}	-22.930	-17.7057
μ_y	0.258	-0.010	β_{yyy}	-2.621	-2.4814
μ_z	0.003	0.002	β_{zzz}	0.001	0.0011
μ	0.916	0.913	β_{xyy}	7.389	5.0916
α_{xx}	-48.860	-51.324	β_{xxy}	-4.815	-6.3932
α_{yy}	-64.119	-65.314	β_{xxz}	0.029	0.0231
α_{zz}	-70.249	-71.970	β_{xzz}	-2.205	-1.7721
α_{xy}	-3.102	-2.655	β_{yzz}	-4.745	-5.8202
α	-61.076	-62.870	β_{yyz}	0.004	0.0038
$\Delta\alpha$ (esu)	392.81905×10^{-25}	354.28708×10^{-25}	βtot(esu)	6.018839×10^{-30}	4.362984×10^{-30}

The correlation equations between these thermodynamic properties and temperatures were fitted by parabolic formula. All the thermodynamic data provide helpful information for the further study on the title compound. From the Table 6. it

Table 6. Statistical thermodynamic parameters of NN dimethyil-m-anisidine at various temperatures.

Temp	Thermodynamic parameters (k cal mol^{-1})			
(Kelvin)	Cp	$(H^o - E^o_o)/T$	$(G_o - E^o_o)/T$	S
100	23.131	11.462	-63.920	75.382
200	35.255	20.919	-76.689	97.607
300	47.918	32.782	-86.915	119.697
400	60.270	46.022	-96.035	142.056
500	71.199	60.253	-104.521	164.774
600	80.456	75.272	-112.552	187.824
700	88.232	90.941	-120.204	211.146
800	94.782	107.157	-127.519	234.677
900	100.320	123.835	-134.526	258.361
1000	105.018	140.907	-141.246	282.154

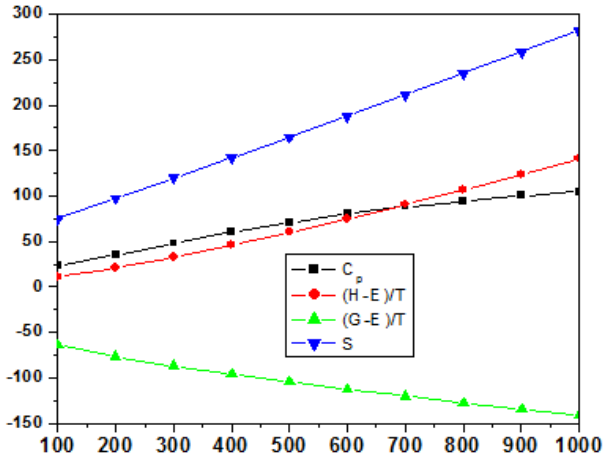

Fig 7. Correlation graph of Gibb's energy, entropy and enthalpy with temperature of NN dimethyil-m-anisidine.

Can be observed that the thermodynamic parameters are increasing expect gibb's free energy with temperature ranging from 100K to 1000K, (Fig. 7) due to the fact that the vibrational intensities of molecule with temperature. From the optimized structure equations are used to predict approximately the values of heat capacity at constant pressure, entropy and internal energy for other range of temperature. The regression coefficient is also given in the parabolic equation.

For DFT

$$C_p = 7.096 + 0.156T - 6.0\times10^{-5}T^2 \quad (R^2 = 0.999)$$

$$(H - E)/T = -0.047 + 0.099T + 4.0\times10^{-5}T^2 \quad (R^2 = 0.999)$$

$$(G - E)/T = -53.76 - 0.116T + 32.0\times10^{-5}T^2 \quad (R^2 = 0.999)$$

$$S = 53.71 + 0.216T + 1.0\times10^{-5}T^2 \quad (R^2 = 1.000)$$

5. Conclusions

Attempts have been made in the present work for the proper frequency assignments for the NNDMA from the FT-IR and FT-Raman spectrum. The observed and the calculated frequencies are in good agreement. The title compound is investigated and analyzed the effect of ionization in the optimized geometries, bond order with the aid of medium level DFT calculations. Ionization causes a small change in the optimized geometry but significant change in the thermodynamic functions of the neutral I3A. The neutral and charged species of second order perturbation analysis shows remarkable deviations after ionization. The DFT-B3LYP/6-311++G(d) calculations have been found more reliable calculations for the vibrational study of NNDMA.

References

[1] M. Aldissi,in: Proceedings of the International Conferenceof Science and Technology of Synthetic Metals (ICSM 88), Santa-Fe, NM, USA, 26 June–2 July 1988, Forward, Synth.Met. 27 (December (1–2)) (1988) AR13–AR14.

[2] A. Skotheim, Handbook of Conducting Polymers, Marcel Dekker, New York, 1987.

[3] D. Sazou, Synth. Met. 130 (2002) 45–54.

[4] E.W. Paul, A.J. Ricco, M.S. Wrighton, J. Phys. Chem. 89 (1985) 1441–1447.

[5] H. Shinohara, T. Chiba, M. Aizawa, Sens. Actuators 13 (1988) 79–86.

[6] Q. Qin, J. Tao, Y. Yang, Synth. Met. 160 (2010) 1167–1172.

[7] A.J. Epstein, J.A.O. Smallfield, H. Guan, M. Fahlman, Synth. Met. 102 (1999) 1374–1376.

[8] S. Patil, J.R. Mahajan, M.A. More, P.P. Patil, S.W. Gosavi, S.A. Gangal, Polym. Int. 46 (1998) 99–105.

[9] L.H. Dao, M. Leclerc, J. Guay, J.W. Chevalier, Synth. Met. 29 (1989) 377–382.

[10] S.F. Patil, A.G. Bedekar, R.C. Patil, J.A.J. Kher, Mater. Sci. 32 (1997) 783–787.
[11] P.A. Kilmartin, G.A. Wright, Synth. Met. 104 (1999) 145–156.
[12] A.A. Athawale, S.F. Patil, B. Deore, Polymer 40 (1999) 4929–4940.
[13] J. Chevalier, J. Bergeron, L.H. Dao, Macromolecules 25 (1992) 3325–3331.
[14] D.S. Lin, S.M. Yan, Synth. Met. 119 (2001) 111–112.
[15] M. Shabani-Nooshabadi, S.M. Ghoreishi, M. Behpour, Electrochim. Acta 54 (2009) 6989–6995.
[16] V. Karpagam, S. Sathiyanarayanan, G. Venkatachari, Curr. Appl. Phys. 8 (2008), 93–98.
[17] A. Olad, A. Rashidzadeh, Prog. Org. Coat. 62 (2008) 293–298.
[18] A. Cook, A. Gabriel, D. Siew, N. Laycock, Curr. Appl. Phys. 4 (2004), 133–136.
[19] P. Ocon, A.B. Christobal, P. Herrasti, E. Fatas, Corros. Sci. 47 (2005) 649–662.
[20] K. Kamaraj, S. Sathiyanarayanan, G. Venkatachari, Prog. Org. Coat. 64 (2009) 67–73.
[21] K.G. Conroy, C.B. Breslin, Electrochim. Acta 48 (2003) 721–732.
[22] S.M.Ghoreishi ∗, M. Shabani-Nooshabadi, M. Behpour, Y. Jafari,
[23] N.C. Handy,C.w.Murray, R.D.Amos, J.Med. Chem. 97 (1993) 4392-4396.
[24] P.J. Stephens, F.J.Derlin, C.F.Charalowski,M.F.Frisch, J.Phys.Chem.98(1994)11623-11627.
[25] F.J.Delvin,J.W.Finley.P.J.Stephens, M.F. Frish,J.Phys.Chem.99(1995)16883-16902.
[26] S.Y.Lee,B.H.Boo,Bull,Kor.J.Chem.Soc.17(1996)760-764.
[27] Progress in Organic Coatings 74 (2012) 502– 510
[28] Gaussian 09, Revision A.1, M. J. Frisch, G. W. Trucks, H. B. Schlegel, G. E. Scuseria, M. A. Robb, J. R. Cheeseman, G. Scalmani, V. Barone, B. Mennucci, G. A. Petersson, H. Nakatsuji, M. Caricato, X. Li, H. P. Hratchian, A. F. Izmaylov, J. Bloino, G. Zheng, J. L. Sonnenberg, M. Hada, M. Ehara, K. Toyota, R. Fukuda, J. Hasegawa, M. Ishida, T. Nakajima, Y. Honda, O. Kitao, H. Nakai, T. Vreven, J. A. Montgomery, Jr., J. E. Peralta, F. Ogliaro, M. Bearpark, J. J. Heyd, E. Brothers, K. N. Kudin, V. N. Staroverov, R. Kobayashi, J. Normand, K. Raghavachari, A. Rendell, J. C. Burant, S. S. Iyengar, J. Tomasi, M. Cossi, N. Rega, J. M. Millam, M. Klene, J. E. Knox, J. B. Cross, V. Bakken, C. Adamo, J. Jaramillo, R. Gomperts, R. E. Stratmann, O. Yazyev, A. J. Austin, R. Cammi, C. Pomelli, J. W. Ochterski, R. L. Martin, K. Morokuma, V. G. Zakrzewski, G. A. Voth, P. Salvador, J. J. Dannenberg, S. Dapprich, A. D. Daniels, Ö. Farkas, J. B. Foresman, J. V. Ortiz, J. Cioslowski, and D. J. Fox, Gaussian, Inc., Wallingford CT, 2009.
[29] G. Rauhut, P. Pulay, J. Phys. Chem. 99 (1995) 3093-3100
[30] P. Pulary, G. Fogarasi, G. Pongor, J.E. Boggs, A. Vargha, J.Am. Chem. Soc. 105 (1983) 7037−7047.
[31] T. Sundius. J.Mol. Struct. 218 (1990) 321−326.
[32] T. Sundius, Vib. Spectrosc. 29 (2002) 89□95.
[33] T. Sundius, Molvib (V7.0): Calculation of harmonic force fields and vibrational modes of molecules, QCPE program No: 807, 2002.
[34] P.L. Polavarapu, J. Phys. Chem. 94 (1990) 8106−8112.
[35] G. Keresztury, S. Holly, J. Varga, G. Besenyei, A.V. Wang, J.R. Durig, Spectrochim. Acta 49A (1993) 2007-2017.
[36] G. Keresztury, in: J.M. Chalmers and P.R. Griffiths (Eds), Handbook of Vibrational Spectroscopy vol.1, John Wiley & Sons Ltd,2002.
[37] R.A. Kydd, S. Mah, Spectrochim. Acta. 38A (1982) 1031-1034.
[38] V. Balachandran, A. Lakshmi, A. Janaki, J. Mol. Struct. 1006, 2011, 395−401
[39] V. Balachandran, T. Karthick, S. Perumal, A. Nataraj, Spectrochim. Acta 92A, 2012, 137−147
[40] G. Santhi, V. Balachandran, V. Karpagam, Elixir Vib. Spec. 36, 2011, 3373−3387.
[41] V. Krishnakumar, N. Prabavathi, Spectrochim. Acta Part A 71, 2008, 449–457.
[42] A. Altun, K. Golcuk, M. Kumru, J. Mol. Struct. (Theochem.), 155, 2003, 637–639.
[43] G. Varsanyi, Vibrational Spectra of Benzene Derivatives, Academic Press, New York, 1969.
[44] Donald L. Pavia, Gary M. Lampman, George S. Kriz, James A.Vyvyan, Introduction to Spectroscopy, Jam Publisher, United States, 2008.
[45] F.R. Dollish, W.G. Fateley, F.F. Bentely, Characteristic Raman Frequencies on Organic Compounds, John Wiley, New York, 1997.
[46] M. Silverstein, G. ClaytonBassler, T.C. Morril, Spectroscopic Identification of Organic Compounds, John Wiley, New York, 1991.
[47] L J Bellamy, The Infrared Spectra of Compound Molecules, Chapman and Hall, London, 1975.
[48] N B Colthup; L H Daly; S E Wiberley, Introduction to Infrared and Raman Spectroscopy, Academic Press Inc., London, 1964.
[49] A M Huralikoppi, Investigation on the spectra of some substituted aromatic molecules; Ph.D thesis, Department of Physics, Karnataka University Dharrwad, 1995.
[50] S. Saravanan, V. Balachandran, Spectrochim. Acta 120A , 2014, 351−364.
[51] V. Krishnakumar, V. Balachandran, Spectrochim. Acta 61A, 2005, 1001–1006.
[52] K.C. Medhi, R. Barman, M.K. Sharma, Indian J. Phys. 68B (2), 1994, 189−190.
[53] B. Smith, Infrared Spectral Interpretation, A Systematic Approach, CRC Press, Washington, DC, 1999.
[54] D.N. Sathyanarayana, Vibrational Spectroscopy—Theory and Applications, second ed., New Age International (P) Limited Publishers, New Delhi, 2004.
[55] J. H. H. Green, D. J. Harrison, W. Kynaston, Spectrochim. Acta 27A, (1971) 2199–2219.
[56] M. Jag, Organic Spectroscopy- Principles and Applications (2nd edition), Narosa Publishing House: New Delhi (2001).
[57] V.K. Rastogi, M.A. Palafox, R.P. Tanwar, M. Lalit, Spectrochim. Acta. part A 58, (2002) 1987–2004.
[58] A. E. Reed, R. B. Weinstock, and F. Weinhold, J. Chem. Phys. 83 (1985)735−746.
[59] P. Politzer, D.G. Truhlar, Eds. Chemical applications of atomic and molecular electrostatic potentials, plenum press, New York, 1981.
[60] A. Srivastava, P. Tandon,S. Jain, B.P. Asthana, Spectrochim. Acta Part A 84 (2011) 144– 155.
[61] D.A. Kleinman, Phys. Rev. 126 (1962) 1977–1979.